ACS APPLIED MATERIALS & INTERFACES

Research Article

www.acsami.org

# Crystalline Transformation of Colloidal Nanoparticles on Graphene Oxide

Chaewon Pak and Doh C. Lee*

Department of Chemical and Biomolecular Engineering, KAIST Institute for the Nanocentury (KINC), Korea Advanced Institute of Science and Technology (KAIST), Daejeon 305-701, Korea

**ABSTRACT:** Emergence of novel two-dimensional (2-D) templates, e.g., graphene oxide, has signified new intriguing opportunities to couple nanocrystals electronically to the microscopic 2-D contacts. A promising approach to uniform dispersion of inorganic nanocrystals on the 2-D interfaces is to graft them through chemical bonding. The 2-D dispersion would offer a unique opportunity to address one of the primary challenges in the field of nanotechnology: fulfilling excellent chemical and physical properties of the nanocrystals in electronic solid-state devices. In this study, we blended colloidal nanocrystals with graphene oxide in aqueous solution in attempts to bind the nanocrystals on reactive sites of the graphene oxide surface, thereby achieving uniform loading. Interestingly, the nanocrystals undergo significant crystalline transformation even under relatively moderate reaction conditions. The growth of particle size and the drastic crystalline deformation, e.g., from wurtzite CdSe to amorphous Se, appear to take place in the proximity of acidic functional groups on graphene oxide. Photocarriers also play a key role in the reaction: under room light, the transformation yielded dramatic size increase and crystalline transformation, whereas in the dark, the change was suppressed. The experimental results presented in this study provide guidelines for uniform 2-D loading of colloidal nanocrystals on graphene oxide. The findings suggest that the surface acidity be titrated for colloidal nanocrystals to deposit on the graphitic layer and to avoid unwanted changes of nanocrystal size and properties.

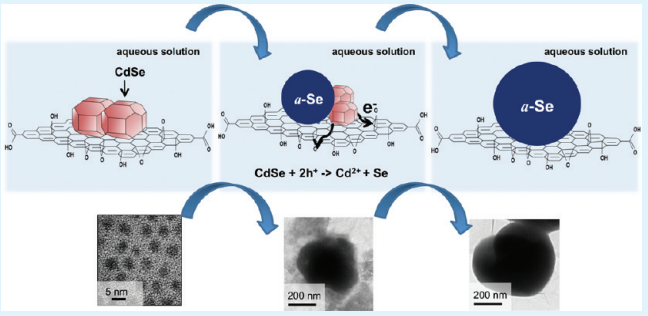


**KEYWORDS:** *graphene oxide, colloidal nanocrystals, hybrid and composite materials, transformation*

## INTRODUCTION

Colloidal inorganic nanocrystals (NCs) of controlled size and shape exhibit a broad range of unique properties.[1] Remarkable progress in synthesis of NCs with uniform size and morphology has sparked the research on the use of these NCs in device applications. For example, growing interest in photovoltaic conversion has driven numerous research groups to experimental efforts to design hybrid materials that can facilitate the transfer of photoinduced charge carriers from nanoscale particles to a more conducting channel, for example, nanowires. Recently, a branch of the research efforts has highlighted the use of graphene, a monolayer of carbon atoms with a two-dimensional (2-D) honeycomb lattice.[2] Despite the ultrahigh conductivity and mechanical strength, blending graphene with NCs remains a challenge, as the attachment of NCs on the graphene surface relies primarily upon the weak van der Waals attraction. One alternative promising approach is to utilize graphene oxide (GO), a graphite sheet chemically functionalized with carboxylic acid at the edges and hydroxyl and epoxide groups mainly on the basal plane. These functional groups help GO exfoliate to form a stable suspension in polar solvent, for example, water.[3] In addition, the functionality enables the anchoring of NCs on the 2-D interfaces either covalently or noncovalently using chemical reaction or electrostatic attraction.[4−6] Although the oxygen-rich moieties reduce charge carrier mobility on GO in comparison to that on graphene, the electronic properties can be restored by chemical,[7−9] thermal,[10] or electrochemical reduction.[11,12]

GO also exhibits large surface area that can be useful in supporting a large number of NCs per layer. On account of the size-tunable properties of semiconductor and metal NCs, the GO−NC and reduced GO (RGO)−NC hybrid structures would offer many exciting opportunities to solve important problems in optoelectronic applications. Especially, 2-D dispersion of semiconductor NCs with controlled size and shape on a GO layer would provide powerful implications for efficient transport of photoinduced charges to targeting electrodes or reaction sites for their use in photocatalysis, light energy conversion, and sensors.[13−19] Since GO is insulating because of its surface functional groups, its reduced version (RGO) would be more useful in the above-mentioned electronic applications. However, using RGO has its own drawbacks: (1) suspending RGO in a solvent is difficult and, more importantly, (2) anchoring NCs on RGO with a sufficient

**Received:** November 28, 2011
**Accepted:** January 5, 2012
**Published:** January 5, 2012

coverage is challenging. One approach to bypass the issues is first to anchor NCs on GO and then to reduce the entire composite via a chemical method.

For integration of the two very exciting classes of materials, NCs and GO, the interactions on the surface of GO should be rigorously investigated. Central to the successful synthesis of NC/GO hybrid structures is to identify reaction conditions that yield uniform 2-D loading of NCs on the GO surface and to investigate the charge and energy transfers between NCs and GO. Current gaps in understanding on interfacing NCs with 2-D templates can be addressed through a study of chemical bonding of the two materials.

In this Article, we study the interaction of colloidal inorganic NCs and GO and discover that NCs undergo significant crystalline transformation even under moderate reaction conditions. For example, when we blend CdSe NCs with GO in aqueous solution for 12 h, the NCs undergo considerable size increase (from 3.6 nm to ∼200 nm) and the crystalline transformation (from wurtzite CdSe to amorphous Se). The formation of the amorphous Se globules indicates that GO promotes the cleavage of Cd−Se bonding and turns the structure into Se. We also monitored morphology changes and compositional transformation in PbSe, $CoPt_3$, and Co NCs in GO-containing aqueous solutions. Electron microscopy and X-ray diffraction data reveal that the transformation occurred in different ways for the different types of NCs. We identified reaction conditions, pH or concentration, which allow nanocrystals to deposit on the GO surface in uniform 2-D dispersion.

## EXPERIMENTAL SECTION

**Materials.** The following chemicals were used as received: graphite (Kropfmühl AG, 99.5%), sulfuric acid ($H_2SO_4$, Aldrich, 99%), phosphorus pentoxide ($P_2O_5$, Aldrich, 99.99%), potassium permanganate (KMnO4, Aldrich, >99%), potassium persulfate ($K_2S_2O_8$, Aldrich, 99.99%), hydrogen peroxide ($H_2O_2$, Aldrich, 30%), hydrochloric acid (HCl, Aldrich, 37%), cadmium oxide (CdO, Aldrich, 99.999%), trioctylphosphine (TOP, Aldrich, 97%), trioctylphosphine oxide (TOPO, Aldrich, 99%), hexylphosphonic acid (HPA, Strem, 99%), lead oxide (PbO, Aldrich, 99.999%), oleic acid (Aldrich, 90%), phenyl ether (99%), di-*i*-butylphosphine (Strem, >97%,), selenium (Se, Aldrich, 99.999%), and 4-aminothiophenol (ATP, TCI, 97%).

**Synthesis of GO.** We prepared graphene oxide (GO) via a modified Hummers method[20,21] by mixing 1 g of graphite flakes with 23 mL of $H_2SO_4$, 0.5 g of $K_2S_2O_8$, and 0.5 g of $P_2O_5$ under ambient conditions for 6 h. The suspension was then dried for 12 h in air after washing with 100 mL of deionized (DI) water. The solid residue (1 g) was transferred to 23 mL of $H_2SO_4$ solution at 0 °C. Three grams of $KMnO_4$ was added to the mixture under mild stirring while the temperature was kept below 20 °C. After 2 h of stirring at 35 °C, we added 46 mL of DI water, and 15 min thereafter, we added 2 mL of $H_2O_2$, upon which the mixture turned bright yellow. We washed the yellow suspension with 10% HCl aqueous solution in order to remove residual metal ions and repeated washing steps with DI water. Finally, the dispersion in water underwent sonication at 300 W for 1.5 h; at this step, GO was exfoliated, and unexfoliated graphite flakes were removed via centrifugal precipitation.

**Synthesis of CdSe, PbSe, $CoPt_3$, and Co NCs.** We synthesized CdSe NCs via a previously reported method.[22] We first prepared Cd−oleate complexes by charging CdO (0.0514 g), HPA (0.1332 g), and TOPO (3.78 g) in a three-neck flask and heating the mixture to 305 °C under Ar, when the mixture turned optically clear. The reaction flask was cooled to 270 °C, at which 0.2 M TOP−Se solution (0.041 g of Se powder dissolved in 3 mL of TOP) was rapidly injected. The temperature of the reaction dropped to 250 °C, and the heating mantle was removed 90 s after injection to cool to room temperature. The "arrested precipitation" approach was also exploited to the synthesis of colloidal PbSe NCs.[23] PbO (0.65 g), oleic acid (2.7 mL), and phenyl ether (4 mL) were loaded in a round-bottom flask and heated to 150 °C under Ar. This clear solution was cooled to 140 °C, and 2 M TOP−Se solution (0.316 g of Se powder dissolved in 2 mL of TOP) was injected. After 60 s, we quenched the reaction by immersing the flask into an iced water bath, and the product was washed with methanol three times. We also prepared colloidal $CoPt_3$[24] and Co NCs[25] via similar wet-chemical methods.

**Ligand Exchange.** As-synthesized NCs dissolve in nonpolar solvents, and in order to dissolve them in water, hydrophobic functional groups, TOPO, HPA, or oleic acid on the inorganic NCs should be removed and replaced with a hydrophilic functionality, such as ATP. We added the solution of ATP (0.626 g) in methanol (10 mL) to a CdSe NC solution in hexane and then stirred the mixture at 40 °C.[5] The CdSe NCs slowly transferred into the methanol phase, and after 24 h of stirring, the NCs were collected through centrifugation at 4000 rpm for 10 min. The powder product was washed with methanol to remove free-floating ATP.

**Preparation of GO/NCs Composite.** The NCs now passivated with ATP (e.g., CdSe−ATP) were soluble in methanol and could blend with GO dispersed in methanol/water without noticeable phase separation. A total of 10 mg of GO and 0.5 mg of CdSe−ATP were mixed in 20 mL of methanol/water mixture (6:1 in methanol/water volumetric ratio). The mixture was stirred for 12 h with room light or in the dark. The final product was washed and then dispersed in DI water. The pH was varied from 4 to 10 by adding diluted $H_2SO_4$ and KOH.

**Characterization.** High-resolution transmission electron microscopy (HRTEM, Philips Tecnai F20 (300 K)), scanning electron microscopy (SEM, FEI Nova230), X-ray photoelectron spectroscopy (XPS, Sigma Probe), and energy dispersive X-ray spectroscopy (EDX) were the primary equipment for characterization of morphology and composition of products. A UV/vis spectrometer (Shimadzu UV3600) was used to measure optical absorbance and an X-ray diffractometer (XRD, D/MAX-IIIC (3 kW)) to investigate the crystalline structure of materials. A Xe lamp (Ocean Optics, HPX-2000, 35 W) was used as a light source in an experiment to see the effect of light on the composite formation. Fourier transform infrared (FTIR) spectra were recorded with an Alpha FT-IR spectrometer to study the changes in the surface functionalities. Photoluminescence (PL) emission spectra were recorded with a HORIBA FL3-2IHR spectrometer.

## RESULTS AND DISCUSSION

CdSe NCs (3.6 nm) coated with 4-aminothiophenol (ATP) have positive surface charge, as an amino group of ATP is positively charged at pHs lower than 8.[26] The positive charge on the surface can interact electrostatically with electron-rich functional groups on the surface of GO. The oxygen-containing functional groups, such as carboxylic, epoxide, hydroxyl, and ketonic moieties, not only keep GO dispersed in water but also serve as active sites which attract the positively charged NCs in their neighborhood.[7,27] For this reason, one can anticipate uniform loading of such positively charged NCs on GO, whose surface features relatively uniform, electronegative functional groups. To our surprise, when ATP-capped CdSe NCs were mixed and stirred with GO in methanol/water mixture for 12 h, the NCs underwent enormous size change: from 3.6 nm to ∼200 nm. Figure 1 shows electron microscopic images and elemental analysis of the product from the blend. HRTEM reveals the transformation of CdSe NCs (Figure 1a) to large globules formed after the blending (Figure 1b) and indicates that the large particles are amorphous, which is also supported by XRD data in Figure 1d. The XRD pattern of the product shows a broad peak at around $2\theta = 20-30°$ corresponding to a-Se.[28] XRD analysis for the CdSe NC samples before and after

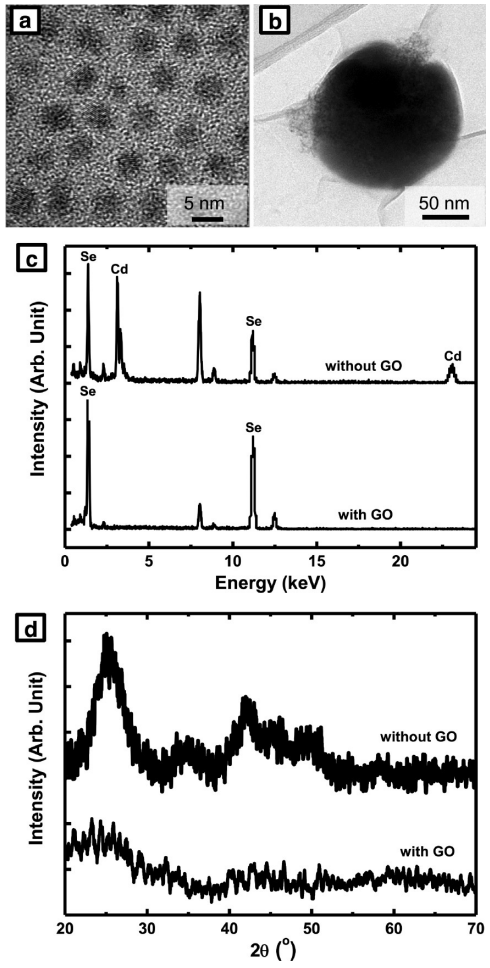


**Figure 1.** TEM images of (a) CdSe–ATP NCs and (b) product collected after mixing with GO for 12 h. (c) EDX spectra of (top) CdSe–ATP and (bottom) GO/CdSe–ATP after stirring for 12 h. It shows the disappearance of Cd signal in the presence of GO. Peaks at ~8 and 9 keV are characteristic of Cu, detected from TEM grids. (d) Powder XRD patterns of product after stirring CdSe–ATP in water without GO (top) and with GO (bottom). CdSe peaks appear in the sample stirred without GO in the mix, whereas a broad peak at ~25° from the sample after stirring with GO indicates amorphous selenium is formed.

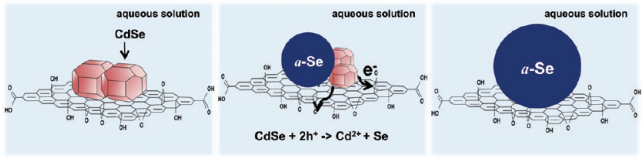


**Figure 2.** Schematic illustration of transformation of CdSe NCs to an a-Se particle on a GO surface.

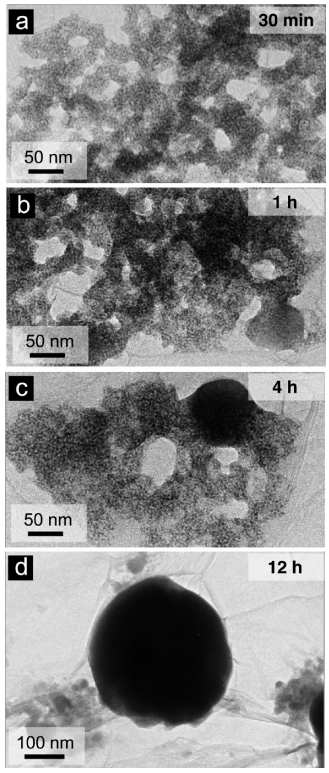


**Figure 3.** TEM images of GO/CdSe–ATP samples taken at different blending times at pH 4. EDX analysis on the imaged area showed decreasing Cd ratio in the sample. Cd:Se was (a) 41:59, (b) 34:66, (c) 10:90, and (d) 1:99.

the blending with the GO solution clearly shows that the peaks for the wurtzite CdSe crystal disappeared after the procedure.

Another stark contrast to the starting CdSe NCs is that the micrometer-sized particles are Se-rich and almost no trace of Cd was detected from EDX spectroscopy from both SEM and TEM analyses. We confirmed that $Cd^{2+}$ ions diffuse out of the GO–CdSe blend from the presence of the dissolved $Cd^{2+}$ in the supernatant. In a control experiment, we stirred ATP-capped CdSe NCs (CdSe–ATP) in the same solvent without GO, and the NCs remained crystalline after 12 h or stirring and the composition of Cd and Se was 55:44 according to EDX results, and the Se deficiency is attributed to the binding of anionic ligand on the surface of the NCs as described in ref 29. Diffusion of $Cd^{2+}$ out of the crystals and the subsequent growth of a-Se particles are illustrated in Figure 2.

We investigated the formation of a-Se particles by taking samples at different reaction times while GO and CdSe–ATP were mixed at pH 4. As shown in Figure 3, CdSe NCs form larger clusters 30 min after the stirring, and after 1 h of reaction, clumping appear to occur more significantly. The EDX analysis of these two samples shows the overall decrease of Cd composition over reaction progress, implying that Cd ion diffusion occurs while clusters grow larger. It is also noteworthy that the Cd composition changed when different regions in the imaged area were checked. This indicates that Cd diffusion takes place as Se-rich clusters form. After 4 h of mixing, large a-Se globules grew around the clusters of CdSe NCs, as if CdSe NCs served as a Se feedstock for the amorphous particle growth. The Cd:Se ratio again decreases as revealed in EDX analysis until eventually no Cd was found in the EDX spectrum of the sample taken at 12 h, supporting our conjecture that the diffusion of $Cd^{2+}$ occurs while a-Se particles form.

Obviously, the transformation of CdSe NCs into a-Se particles would involve the breaking of the Cd–Se bonding in the crystal, and our experimental data indicate that GO plays a critical role in the cleavage of the bonding. We observed that GO turns the solution acidic[30] due to the release of protons from acidic sites (for example, carboxylic and alcohol groups) and FT-IR spectra of GO reveal the existence of such functional groups on the surface (Figure 4). For the concentration of GO used in the blending experiment (1 mg/mL), the solution


dx.doi.org/10.1021/am201666q | ACS Appl. Mater. Interfaces 2012, 4, 1021–1029

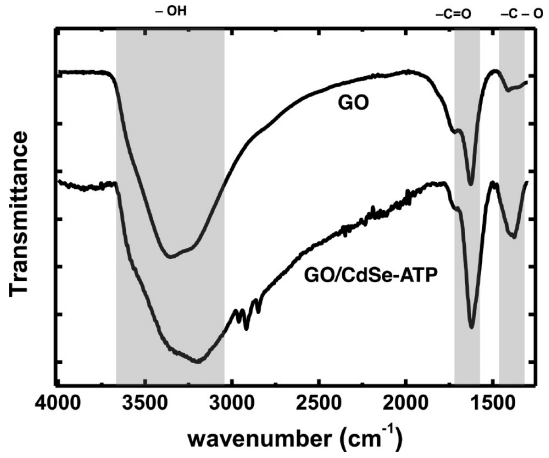


**Figure 4.** FT-IR spectra of GO and GO/CdSe–ATP. GO exhibits the characteristic bands including O—H stretch at 3500–2500 $cm^{-1}$, C═O stretch at 1700 $cm^{-1}$, and C—O stretch at 1300–1000 $cm^{-1}$. C—H stretch at ~2800 $cm^{-1}$ results likely from the remaining TOPO ligands on the surface of CdSe NCs.

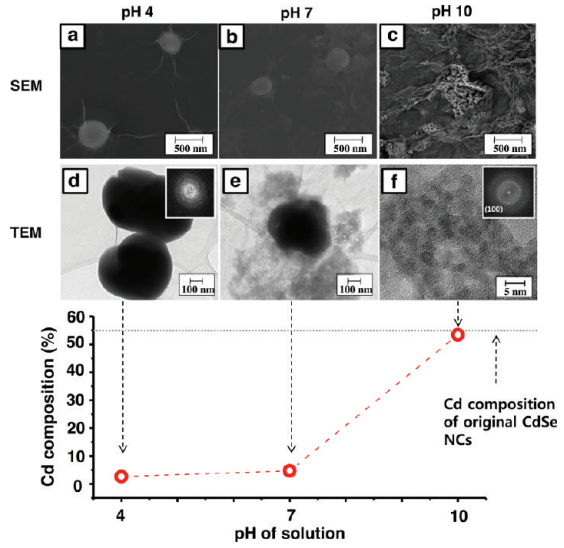


**Figure 5.** SEM (a–c) and TEM (d–f) images of product collected after mixing GO and CdSe–ATP for 12 h at pH 4 (a, d), 7 (b, e), and 10 (c, f). (bottom) Plot of Cd composition of the product after the mixing as a function of the pH of the solution.

showed pH at 4.5. The value is in agreement with previous studies on chemical properties of GO.[30,31] We hypothesized that GO turns the solution acidic, and at the lowered pH, the standard potential for the Cd–Se bond formation decreases. To test this hypothesis, we investigated the possibility that the acidity plays a key role in the transformation by carrying out the blending experiments at different pH with GO in the mix. In fact, previous studies illustrate increased Cd release from CdSe NCs in acidic aqueous solutions, and the studies discuss possible cytoxicity of CdSe NCs particularly for some organs with an innate acidic environment, for example, the stomach.[32−35] We observed the increase in pH of the blending mixture as the GO/CdSe–ATP mixing proceeded: a similar pH change was observed by Xi et al.,[36] who reported that light can induce the generation of charges in CdSe nanocrystals. They observed that, under aqueous environment, some of these charges undergo reactions with water to form hydroxide ions, thereby increasing the pH of the entire solution. The FT-IR spectra shown in Figure 3 indicate no noticeable reduction of GO; however, the photogenerated electrons can instead be transferred to water in the way of forming hydroxide ions.

The detachment of thiolate typically accompanies the release of Cd ions. Figure 5 shows the results of mixing ATP-capped CdSe (CdSe–ATP) NCs and GO for 12 h in solutions with different pH values ranging from 4 to 10. At pH 4, SEM and HRTEM images and EDX analysis reveal that the product consists mostly of large a-Se globules sitting on wrinkled graphene oxide layers, and the FFT of the TEM image (inset, Figure 5d) clearly shows the amorphous nature of the product. It is likely that when the NCs were blended with GO, the acidic environment reduced the standard potential for the particle formation and resulted in the cleavage of the Cd–Se bonding. Then, $Cd^{2+}$ ions, which diffused out of the CdSe crystal lattice, would remain in solvent. EDX analysis confirms that the supernatant is indeed Se-free and Cd-rich (atomic ratio Cd:Se = 9:1).

When the reaction of CdSe–ATP and GO is carried out at elevated pH, the transformation occurred to a smaller degree. For example, at pH 7, a-Se globules and clusters of <10 nm-sized CdSe NCs are both found from the mixture, and at pH 10, large particles (over 100 nm) were not found and CdSe NCs appear to retain their size during the blending. Figure 5b,e shows SEM and TEM images of the product from the pH 7 experiment, and it is apparent that CdSe NCs are frequently found around the large a-Se particles as if CdSe NCs acted as feedstock for the Se supply for the growth of the globule. At pH 10, CdSe NCs appeared to flocculate, but the HRTEM analysis at high magnification indicates that NCs retained their original size and crystallinity (Figure 5f). Passivaion of CdSe NCs with ATP is relatively weak, and stirring causes the NCs to cluster, as ATP molecules begin to detach from the NC surface. From the pH dependence investigation, it is evident that the acidity of the solution is one of the important parameters in the transformation of CdSe NCs into larger amorphous Se particles. If the acidity were an only component, CdSe–ATP NCs would completely transform into a-Se particles at low pH regardless of the presence of GO in the mix.

However, when we carried out the stirring at varying pH of the solution *without GO*, the transformation did not appear to follow our prediction. For example, even at pH 4, only a small fraction of CdSe NCs transformed to a-Se (Figure 6a). As shown in Figure 6b,c, the transformation did not occur at pH 7–10, when GO was not present in the solution. We should take into account that when GO is present in solution, surface acidity of GO may cause the acidity gradient. In other words, even at identical overall pH of solution (e.g., at pH 4), the mixture containing GO shows stronger acidity near the GO surface. We can infer that the role of GO in the transformation is beyond just acidity because CdSe-to-Se transformation occurs much more significantly in the presence of GO at an identical bulk pH value of the acidic solution.

To gain further insights into the electronic interactions responsible for the dissolution of NCs on the GO surface, we carried out CdSe–ATP NCs/GO blending experiments in bright and dark conditions. We explored the possibility that photogenerated charge carriers or excitons in CdSe NCs influence the transformation reaction on the electron-rich GO surface. Figure 7 shows UV–vis spectra of the sample after mixing CdSe–ATP NCs and GO in room light and in the dark. Under room light, the blending results in blue shift of the 1S

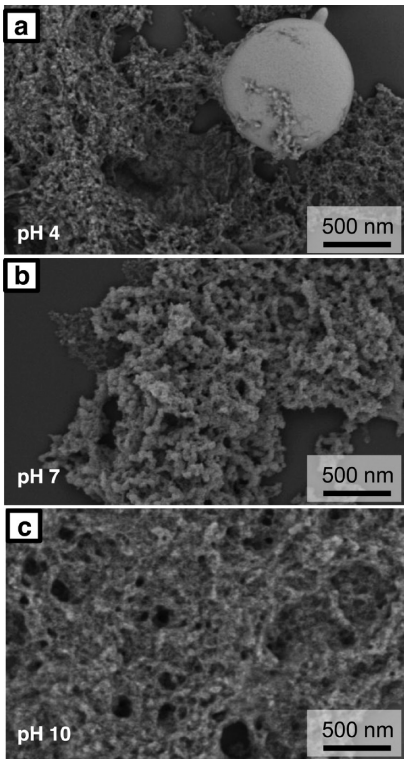


**Figure 6.** SEM images of CdSe–ATP after stirring 12 h without GO at (a) pH 4, (b) pH 7, and (c) pH 10.

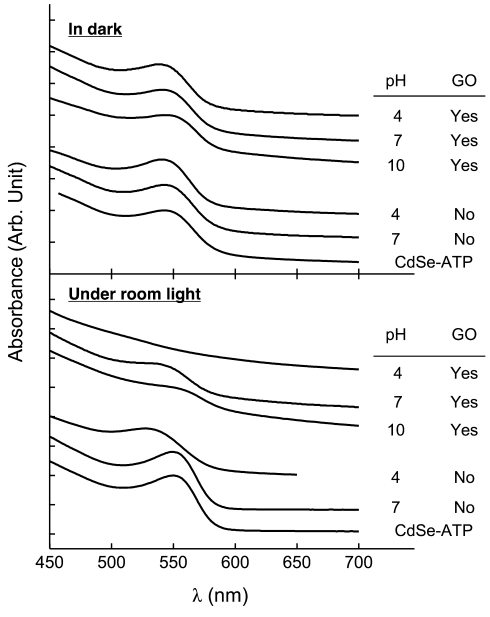


| pH | In dark | | Under light | |
|---|---|---|---|---|
| | GO | w/o GO | GO | w/o GO |
| 4 | 538 nm | 540 nm | no peak | 530 nm |
| 7 | 540 nm | 543 nm | 540 nm | 550 nm |
| 10 | 545 nm | 545 nm | 550 nm | 550 nm |

**Figure 7.** UV–vis absorption spectra of CdSe–ATP and GO/CdSe–ATP at various pH values in the dark and with room light. The blue-shift and disappearance of the first absorption peaks for samples result from the dissolution and transformation of CdSe.

transition peak (~550 nm to ~540 nm) at pH 7 or leads to the disappearance of the 1S peak at pH 4. The shift and disappearance of the 1S peak at different pH values explain the morphological changes observed in electron microscopic images and elemental analysis. In contrast, the 1S absorption peak undergoes almost no shift when the blending was carried out in the dark (Figure 7). SEM and TEM images and the excitonic peak in the absorption spectra indicate that the size of NCs decreases at a mild condition and NCs eventually decompose on the GO surface in a more acidic solution.[36] Cd:Se composition analysis indicates that size and composition of CdSe NCs retain their original values after the blending in the dark condition. We postulate that in the bright condition, CdSe NCs absorb light, produce electron–hole pairs, and provide necessary charges for the redox reaction that converts $Se^{2-}$ to charge-neutral Se. The standard oxidation potentials of $Se^{2-}/Se$ and $H_2/H^+$ are 0.92 and −0.83 V, respectively,[37] and thus the oxidation of $Se^{2-}$ to Se is thermodynamically probable. Hence, the blue shift and disappearance of the 1S excitonic peak in the absorption spectra indicate that the size of NCs decreases at a mild condition and NCs eventually decompose on the GO surface in a more acidic solution.[36]

To confirm that the photocarriers help degrade and transform CdSe NCs, we left the GO/CdSe–ATP mixture under the illumination of a Xe lamp. The reaction progress was indeed accelerated. UV–vis absorption spectra of the blend show that the characteristic CdSe peak decreases rapidly under the Xe lamp illumination (see Figure 8) so the peak nearly

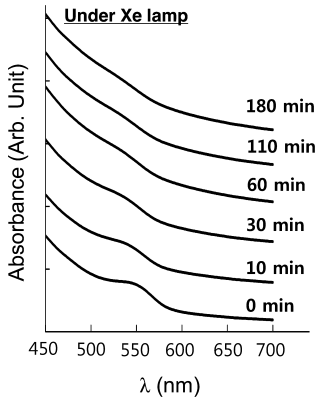


**Figure 8.** UV–vis absorption spectra of GO/CdSe–ATP blended under Xe-lamp illumination for different amounts of time (0 min to 3 h). 1S absorption peak of CdSe NCs at ~550 nm gradually decreased, and after 3 h of reaction, the peak is no longer clearly evident. This is in contrast to the experiment in which the reaction conditions were the same except the light source was room light. In room light, the 1S absorption peak remained visible at longer reaction time.

disappears in 30 min, whereas the peak remained discernible at least for 3 h of reaction time when the blending was under room light. This result clearly shows that light plays a critical role in the transformation of the semiconductor nanocrystals.

GO is composed of graphitic carbon hexagons, with carboxylic groups and other oxygen-containing functionalities. As illustrated in Figure 2, photoinduced charge carriers are trapped in the functional groups on the GO surface and participate in binding the surface of CdSe NCs. Upon tethering of CdSe NCs on the GO surface, photoluminescence (PL) is quenched. When CdSe–ATP NCs are stirred in solution without GO for 4 h, PL intensity dropped by 15%. On the

other hand, with GO in the blend, the quenching of emission is much more significant (71%). This PL quenching indicates considerable charge transfer from CdSe NCs to GO. This is in good agreement with recent reports that electron transfer from quantum dots to graphene is fast.[5] The mean free path of charge carriers is dictated by the surface coverage of oxygen-containing functional groups on GO because of the charge traps induced by oxygen functional groups of GO.[38,39] Therefore, transformation of CdSe NCs into micrometer-sized a-Se globules more readily occurs when the GO surface is enriched with oxygenated functionalities.[40]

We investigated whether the crystalline transformation transpires universally in other alloy structures. Lead chalcogenide NCs are of particular interest because they exhibit a rich library of interesting optical properties that may find intense use in photovoltaics, photodetectors, and solid-state lasing.[41] For example, the study of multiple excitons and their dynamics in PbSe quantum dots has fueled the intrigue in the increased photon energy conversion efficiency by generating more than one electron–hole pair in a NC with a single photon.[42]

We transferred PbSe NCs from nonpolar to aqueous solution via ligand exchange to carry out a similar mixing experiment with GO. The ligand exchange resulted in PbSe NCs passivated with ATP molecules and that dissolved in methanol to which GO solution was added. The ligand-exchanged PbSe NCs (denoted as PbSe–ATP) retain their crystallinity as evidenced in HRTEM images (Figure 9b). For example, the lattice fringes displayed in the HRTEM image in Figure 9b are spaced by 3.1 Å, which corresponds to (200) planes for the rock salt structure of PbSe. After the reaction with GO at pH 4, the PbSe NCs were transformed into much larger crystals as shown in Figure 9c. Also, as shown in the HRTEM image in the inset of Figure 9c, the crystals are PbO with lattice spacing of 3.1 Å and 2.7 Å, which corresponds to the plane spacing of (111) and (200), respectively, with a bisecting angle of 56.1° found in orthorhombic PbO.[43] Interestingly, the transformation also occurred at low pH even if GO was not present in the mixing solution (Figure 9e), although the degree of transformation was smaller than when GO was in the mix. In the case of PbSe NCs, facilitation by GO does not appear to be as dramatic as the case of CdSe NCs, for the crystalline transformation. Apparently, acidity is a critical factor. Although the transformation occurred for PbSe NCs regardless of the presence of GO in acidic solutions, the transformed crystals are larger and have broader size distribution when GO was present (width: from 44 to 270 nm, height: from 74 to 278 nm) whereas rather narrow size distribution appears without GO (about 50 nm by 50 nm). When $H_2SO_4$ was not used for the titration of the solution, this transformation happened only when GO was mixed in the solution, as shown in Figure 9d.

This observation has a clear and direct relevance to the previous results that GO provides local surface acidity. An XRD pattern of PbSe NCs shows the rock salt PbSe peaks, whereas XRD data for the sample collected after the stirring with GO exhibit no such peaks (Figure 10). Instead, characteristic patterns of complex oxides (PbO, $PbSeO_3$, and $SeO_2$) show up.

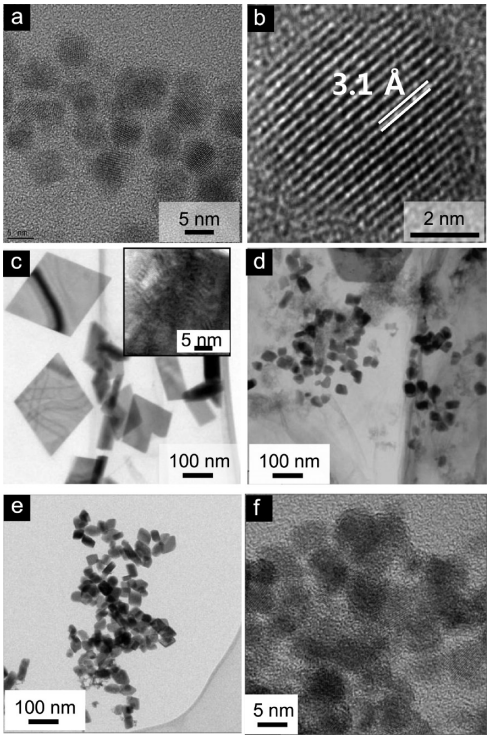


**Figure 9.** (a,b) TEM images of ATP-passivated PbSe NCs. High-magnification image in (b) clearly shows lattice fringes with the spacing of 0.31 nm, (200) plane of rock salt PbSe. (c–f) TEM images of the product collected after mixing PbSe–ATP with GO at (c) pH 4 and (d) pH 7 and without GO at (e) pH 4 and (f) pH 7. The magnified TEM image for the transformed products (inset, c) shows lattice spacing corresponding to lead oxide with orthorhombic structure.

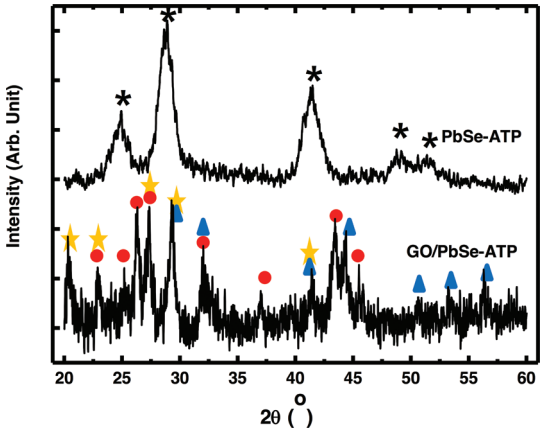


**Figure 10.** Powder XRD patterns of PbSe–ATP (top) and GO/PbSe–ATP (bottom). The symbol of (*) represents the characteristic peaks for the rock-salt structure of PbSe–ATP NCs, and each symbol in the patterns of GO/PbSe–ATP represents the characteristic peaks for PbO (circle), $PbSeO_3$ (triangle), and $SeO_2$ (star).

We also carried out XPS measurements to determine chemical composition and oxidation states of the products. As shown in Figure 11a, we can see that the Pb (4f) in the range between 133 and 148 eV shows two dominant peaks at 138.5 and 143.5 eV. The peak at 138.5 eV is attributed to the Pb(II) state in Pb–O bonding of 138.4 eV rather than Pb–Se bonding of 137.6 eV. This peak position implies the presence of PbO in the sample.[44] We also observe clear signatures of selenium oxidation in the GO treated sample. The Se (3d) XPS spectrum in the range of 49–63 eV shows the signal from the Se 3d level at 55.1 eV, which is broadened due to the presence of two Se features, corresponding to $3d_{5/2}$ and $3d_{3/2}$ levels (Figure 11b). However, binding energy obtained at 55.1 eV is closer to

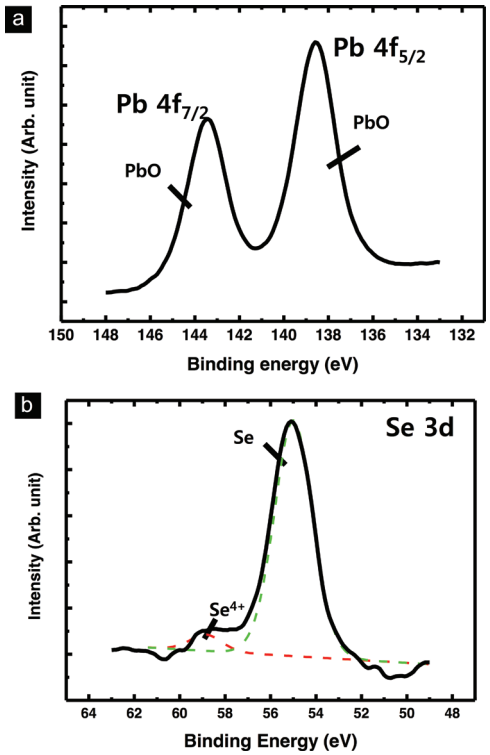


**Figure 11.** XPS data of PbSe NCs after stirring with GO at pH 4 for 12 h. It shows (a) Pb 4f and (b) Se 3d transitions, and the result of spectral fitting (dashed lines) of Se 3d shows the relative contribution of Se chemical states.

neutral Se of 55.3 eV than $Se^{2-}$ in PbSe of 54.2 eV, which indicates the presence of elemental Se dominantly. In addition, a small peak at 59 eV appears, attributed to $Se^{4+}$ in $SeO_2$ or $PbSeO_3$. From the quantitative analysis of XRD and XPS results, the oxide complex of PbSe NCs is present in the ratio of $PbO/Se/PbSeO_3/SeO_2$ 0.97:1:0.016:0.015. These observations are consistent with EDX analysis of the TEM image in Figure 12. It shows the gradual change of the Pb to Se ratio in different

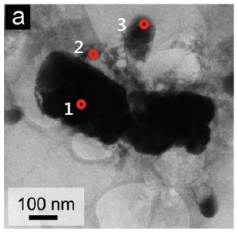


b

| Number | Atomic % | |
|---|---|---|
| | Pb | Se |
| 1 | 91 | 9 |
| 2 | 24 | 76 |
| 3 | 1 | 99 |

**Figure 12.** (a) TEM image of the product collected after mixing PbSe–ATP with GO at pH 4 for 12 h and (b) atomic concentration obtained from EDX analysis for different spots of the product.

spots of the product. Spot 1 is the Pb dominant phase whereas spot 2 is Se rich because after the cleavage of Pb–Se bonding, Pb ions are diffused out from PbSe and subsequently transformed into PbO crystals. It was also found that Se anions left on the GO surface also form a-Se particles nearby (spot 3), so we can conclude oxidation of PbSe proceeds through formation of PbO crystals and a-Se particles. According to XRD and XPS results, traces of $SeO_2$ and $PbSeO_3$ must exist, but they are not distinguishable in TEM images.

The oxidation process of PbSe takes place through a number of different pathways.[45−48] The numerous oxidation processes are described below:

$$PbSe(s) + 2O_2(g) = PbSeO_4(s)$$
$$\Delta G^\circ = -405\ \text{kJ mol}^{-1} \quad \text{at 298 K} \tag{1}$$

$$PbSe(s) + \frac{3}{2}O_2(g) = PbSeO_3(s)$$
$$\Delta G^\circ = -352\ \text{kJ mol}^{-1} \quad \text{at 298 K} \tag{2}$$

$$PbSe(s) + \frac{3}{2}O_2(g) = PbO(s) + SeO_2(s)$$
$$\Delta G^\circ = -262\ \text{kJ mol}^{-1} \quad \text{at 298 K} \tag{3}$$

$$PbSe(s) + O_2(g) = PbO(s) + \frac{1}{2}Se_2(s)$$
$$\Delta G^\circ = -201\ \text{kJ mol}^{-1} \quad \text{at 298 K} \tag{4}$$

$$PbSe(s) + O_2(g) = Pb(s) + \frac{1}{2}SeO_2(s)$$
$$\Delta G^\circ = -74\ \text{kJ mol}^{-1} \quad \text{at 298 K} \tag{5}$$

According to the equilibrium free energies for processes 1–5, $PbSeO_4$ is the thermodynamically most stable compound among the reaction products of the oxidation of PbSe. However, the free energy-based consideration conflicts with recent results on oxidation of PbSe at room temperature. Sykora et al. explained that reaction 1 was kinetically inhibited at room temperature due to an excitation barrier, so oxidation of PbSe NCs proceeds mostly via a combination of 2–4.[47] This explains our experimental results well. However, in our study, the oxidation was facilitated so that not only did the oxides form on the surface of NCs but also the oxidation reaction on the surface of GO results in almost complete oxidation of PbSe NCs, which is supported by TEM, XRD, and XPS analysis. This is in contrast to previous work because it was found that the oxidation process usually occurs just on the surface of NCs. Also noteworthy is that the transformation leads to the formation of both PbO crystals and a-Se particles from the PbSe NCs whereas the similar acidic environment resulted in the ejection of cadmium from CdSe NCs and formation of a-Se particles. This distinction can be explained by the electronegativity difference between PbSe and CdSe. The electronegativity of Se (2.55) is larger than that of Cd (1.69); consequently, the larger charge transfer from Cd to Se is expected in NCs. As oxidation proceeds, dissolved cadmium ion can be rapidly ejected from CdSe due to its smaller ionic radius of Cd (109 pm) than that of Se (184 pm) and subsequently diffuses into solvent. In the case of PbSe, however, Pb has relatively higher electronegativity (2.33) and larger ionic radius (133 pm) than Cd, which induces formation of stable Pb–O bonding rather than removal of Pb. The formation of oxide compounds means Pb–Se bonding is broken, and Se–O, Pb–O, and Se–Se bondings are formed instead. Dissociation energies for the Pb–Se bond (302 kJ) requires less energy to cleave than the Pb–O (378 kJ), Se–Se (333 kJ), and Se–O (464 kJ) ones, so once the Pb–Se bond is cleaved, stable oxidation products such as PbO, Se, $PbSeO_3$,

and $SeO_2$ are formed.[44] The bonding energy for Cd−Se is similar to that of Pb−Se, so after cleavage of Cd−Se bonding, the cadmium ion diffuses into solvent instead of the formation of Cd−O bonding with the much weaker bonding energy (142 kJ).

The same principle can be applied to $CoPt_3$ and Co NCs. The Co−Pt bonding in $CoPt_3$ takes relatively higher energy to break in comparison to Pb−Se and Cd−Se bonds. Therefore, no oxidation products were observed in the case of $CoPt_3$ NCs (Figure 13a,b). On the other hand, Co NCs are oxidized to

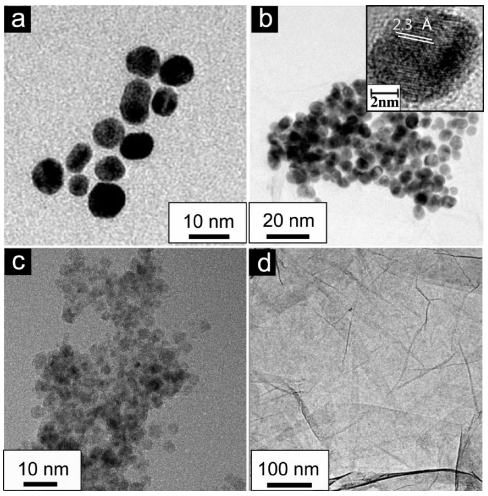


**Figure 13.** TEM images of (a, b) $CoPt_3$ and (c, d) Co NCs before (a and c) and after (b and d) stirring with GO for 12 h.

cobalt ions after the reaction with GO as indicated in TEM images in Figure 13c,d. The oxidation of Co NCs has been discussed previously in reports about the dissolution of cobalt in acidic aqueous media.[49,50] The results point to the possibility that the structural and compositional deformation of various kinds of NCs can be prompted by GO.

## CONCLUSION

Colloidal NCs undergo drastic structural transformation and compositional deformation when they are mixed with GO in aqueous solution. For example, 3.6 nm CdSe NCs turn into a-Se particles of size as large as ∼500 nm, and 6.8 nm PbSe NCs transformed into PbO of size ranging from 50 to 280 nm and other types of oxide complexes. The acidic nature of functional groups on GO is believed to facilitate the cleavage of Cd−Se bondings, and then $Cd^{2+}$ ions, which diffused out of the CdSe crystal lattice, end up in solution. The local acidity of GO caused by the release of protons from acidic sites (for example, carboxylic and alcohol groups) induces acidic condition of the solution, so the standard potential for the Cd−Se bond formation decreases. The functional groups of GO have been reported to immobilize chalcogenide ions, and the anchoring of Se is believed to play a key role in the CdSe-to-Se transformation.[51] We also found that the photon influences the crystalline deformation and transformation. The result is also in accord with a postulation that charge carriers are transferred between NCs and GO efficiently. Crystalline transformation takes place in different fashions in the case of PbSe and Co NCs. The distinction stems from the bonding strength of the different crystals. For example, $CoPt_3$ NCs do not undergo such transformation, which is attributed to high dissociation energy of Co−Pt bonding. Consequently, the series of experimental results indicates that the structural and compositional deformation of various kinds of NCs can be prompted by GO.

Extremely high carrier mobility and long spin transfer length render graphene an attractive template for efficient charge and spin transport channel.[52] For example, if semiconductor nanocrystal quantum dots are tethered on the surface of graphene, a charge carrier with a spin generated in the NCs could be transferred through a pristine graphene layer, as far as exceeding 100 nm even at room temperature.[53] One critical roadblock in making such hybrid structures is the attachment of NCs on graphene, which has no functional moieties to chemically hold NCs. By utilizing GO, we can deposit NCs on its surface, and eventually, the functional groups can be reduced to increase the template's carrier transport efficiency. This study reveals that even a simple blending of NCs and GO in aqueous solution results in significant sintering and crystalline transformation. Through careful titration of local acidic sites on GO, one can achieve uniform dispersion, which is useful for many applications, without damaging the NC morphology and size control. Further investigation on layer-by-layer assembled NC−GO hybrid structures is underway.

## AUTHOR INFORMATION

### Corresponding Author

*E-mail: dclee@kaist.edu.

## ACKNOWLEDGMENTS

This work was supported by the National Research Foundation (NRF) grant funded by the Korean government (MEST) (No. 2011-0030256 and No. 2011-0013441). This research was also partially supported by the High Risk High Return Project (HRHRP) program from the Office of Research Affairs at KAIST. D.C.L. acknowledges the KAIST Startup Fund (Project No. G04100077).

## REFERENCES

(1) Murray, C.; Kagan, C.; Bawendi, M. *Annu. Rev. Mater. Sci.* **2000**, *30*, 545.
(2) Singh, V.; Joung, D.; Zhai, L.; Das, S.; Khondaker, S. I.; Seal, S. *Prog. Mater. Sci.* **2011**, *56*, 1178.
(3) Stankovich, S.; Dikin, D. A.; Dommett, G. H. B.; Kohlhaas, K. M.; Zimney, E. J.; Stach, E. A.; Piner, R. D.; Nguyen, S. T.; Ruoff, R. S. *Nature* **2006**, *442*, 282.
(4) Dreyer, D. R.; Park, S.; Bielawski, C. W.; Ruoff, R. S. *Chem. Soc. Rev.* **2010**, *39*, 228.
(5) Pham, T. A.; Choi, B. C.; Jeong, Y. T. *Nanotechnology* **2010**, *21*, 465603.
(6) Lu, G. H.; Mao, S.; Park, S.; Ruoff, R. S.; Chen, J. H. *Nano Res.* **2009**, *2*, 192.
(7) Li, D.; Muller, M. B.; Gilje, S.; Kaner, R. B.; Wallace, G. G. *Nat. Nanotechnol.* **2008**, *3*, 101.
(8) Compton, O. C.; Nguyen, S. B. T. *Small* **2010**, *6*, 711.
(9) Zhou, X. J.; Zhang, J. L.; Wu, H. X.; Yang, H. J.; Zhang, J. Y.; Guo, S. W. *J. Phys. Chem. C* **2011**, *115*, 11957.
(10) Zhu, Y.; Stoller, M. D.; Cai, W.; Velamakanni, A.; Piner, R. D.; Chen, D.; Ruoff, R. S. *ACS Nano* **2010**, *4*, 1227.
(11) Ramesha, G. K.; Sampath, S. *J. Phys. Chem. C* **2009**, *113*, 7985.
(12) Wang, Z.; Zhou, X.; Zhang, J.; Boey, F.; Zhang, H. *J. Phys. Chem. C* **2009**, *113*, 14071.
(13) Kamat, P. V. *J. Phys. Chem. Lett.* **2009**, *1*, 520.
(14) Cao, A. N.; Liu, Z.; Chu, S. S.; Wu, M. H.; Ye, Z. M.; Cai, Z. W.; Chang, Y. L.; Wang, S. F.; Gong, Q. H.; Liu, Y. F. *Adv. Mater.* **2010**, *22*, 103.

(15) Kim, S. R.; Parvez, M. K.; Chhowalla, M. *Chem. Phys. Lett.* **2009**, *483*, 124.
(16) Wang, Y.; Lu, J.; Tang, L. H.; Chang, H. X.; Li, J. H. *Anal. Chem.* **2009**, *81*, 9710.
(17) Xu, T. G.; Zhang, L. W.; Cheng, H. Y.; Zhu, Y. F. *Appl. Catal. B* **2011**, *101*, 382.
(18) Lin, Y.; Zhang, K.; Chen, W. F.; Liu, Y. D.; Geng, Z. G.; Zeng, J.; Pan, N.; Yan, L. F.; Wang, X. P.; Hou, J. G. *ACS Nano* **2010**, *4*, 3033.
(19) Joung, D.; Singh, V.; Park, S.; Schulte, A.; Seal, S.; Khondaker, S. I. *J. Phys. Chem. C* **2011**, *115*, 24494.
(20) Hummers, W. S.; Offeman, R. E. *J. Am. Chem. Soc.* **1958**, *80*, 1339.
(21) Zhang, L.; Xia, J.; Zhao, Q.; Liu, L.; Zhang, Z. *Small* **2010**, *6*, 537.
(22) Peng, Z. A.; Peng, X. *J. Am. Chem. Soc.* **2001**, *123*, 183.
(23) Pietryga, J. M.; Werder, D. J.; Williams, D. J.; Casson, J. L.; Schaller, R. D.; Klimov, V. I.; Hollingsworth, J. A. *J. Am. Chem. Soc.* **2008**, *130*, 4879.
(24) Tian, Y.; Shen, C.; Li, C.; Shi, X.; Huang, Y.; Gao, H. *Nano Res.* **2011**, *4*, 780.
(25) Puntes, V. F.; Krishnan, K. M.; Alivisatos, A. P. *Science* **2001**, *291*, 2115.
(26) Torimoto, T.; Sakata, T.; Mori, H.; Yoneyama, H. *J. Phys. Chem.* **1994**, *98*, 3036.
(27) Chen, J. S.; Wang, Z. Y.; Dong, X. C.; Chen, P.; Lou, X. W. *Nanoscale* **2011**, *3*, 2158.
(28) Bindu, K.; Lakshmi, M.; Bini, S.; Kartha, C. S.; Vijayakumar, K.; Abe, T.; Kashiwaba, Y. *Semicond. Sci. Technol.* **2002**, *17*, 270.
(29) Deng, Z.; Cao, L.; Tang, F.; Zou, B. *J. Phys. Chem. B* **2005**, *109*, 16671.
(30) Szabo, T.; Tombacz, E.; Illes, E.; Dekany, I. *Carbon* **2006**, *44*, 537.
(31) Pyun, J. *Angew. Chem., Int. Ed.* **2011**, *50*, 46.
(32) Kirchner, C.; Liedl, T.; Kudera, S.; Pellegrino, T.; Javier, A. M.; Gaub, H. E.; Stölzle, S.; Fertig, N.; Parak, W. J. *Nano Lett.* **2005**, *5*, 331.
(33) Derfus, A. M.; Chan, W. C. W.; Bhatia, S. N. *Nano Lett.* **2004**, *4*, 11.
(34) Wang, L.; Nagesha, D. K.; Selvarasah, S.; Dokmeci, M. R.; Carrier, R. L. *J. Nanobiotechnol.* **2008**, *6*, 11.
(35) Aldana, J.; Lavelle, N.; Wang, Y.; Peng, X. *J. Am. Chem. Soc.* **2005**, *127*, 2496.
(36) Xi, L.; Lek, J. Y.; Liang, Y. N.; Boothroyd, C.; Zhou, W.; Yan, Q.; Hu, X.; Chiang, F. B. Y.; Lam, Y. M. *Nanotechnology* **2011**, *22*, 275706.
(37) Tang, Z.; Wang, Y.; Sun, K.; Kotov, N. A. *Adv. Mater.* **2005**, *17*, 358.
(38) Yi, M.; Zhao, L.; Fan, Q.; Xia, X.; Ai, W.; Xie, L.; Liu, X.; Shi, N.; Wang, W.; Wang, Y. *J. Appl. Phys.* **2011**, *110*, 063709.
(39) Joung, D.; Chunder, A.; Zhai, L.; Khondaker, S. I. *Appl. Phys. Lett.* **2010**, *97*, 093105.
(40) Williams, G.; Seger, B.; Kamat, P. V. *ACS Nano* **2008**, *2*, 1487.
(41) Rogach, A. L.; Eychmüller, A.; Hickey, S. G.; Kershaw, S. V. *Small* **2007**, *3*, 536.
(42) Klimov, V. I. *J. Phys. Chem. B* **2006**, *110*, 16827.
(43) Cattley, C. A.; Stavrinadis, A.; Beal, R.; Moghal, J.; Cook, A. G.; Grant, P. S.; Smith, J. M.; Assender, H.; Watt, A. A. R. *Chem. Commun.* **2010**, *46*, 2802.
(44) Gautier, C.; Cambon-Muller, M.; Averous, M. *Appl. Surf. Sci.* **1999**, *141*, 157.
(45) Tomaev, V.; Chernyshova, I.; Tikhonov, P. *Glass Phys. Chem.* **2007**, *33*, 646.
(46) Galat, J.; Haber, J.; Nowotny, J.; Wagner, J. *Oxid. Met.* **1975**, *9*, 497.
(47) Sykora, M.; Koposov, A. Y.; McGuire, J. A.; Schulze, R. K.; Tretiak, O.; Pietryga, J. M.; Klimov, V. I. *ACS Nano* **2010**, *4*, 2021.
(48) Tomaev, V.; Makarov, L.; Tikhonov, P.; Solomennikov, A. *Glass Phys. Chem.* **2004**, *30*, 349.
(49) Soler, M. A. G.; Lima, E. C. D.; da Silva, S. W.; Melo, T. F. O.; Pimenta, A. C. M.; Sinnecker, J. P.; Azevedo, R. B.; Garg, V. K.; Oliveira, A. C.; Novak, M. A. *Langmuir* **2007**, *23*, 9611.
(50) Jiang, H.; Liu, F.; Yang, H.; Li, Y. *Biol. Trace Elem. Res.* **2011**.
(51) Ji, L.; Rao, M.; Zheng, H.; Zhang, L.; Li, Y.; Duan, W.; Guo, J.; Cairns, E. J.; Zhang, Y. *J. Am. Chem. Soc.* **2011**, *133*, 18522.
(52) Bolotin, K.; Sikes, K.; Jiang, Z.; Klima, M.; Fudenberg, G.; Hone, J.; Kim, P.; Stormer, H. *Solid State Commun.* **2008**, *146*, 351.
(53) Berger, C.; Song, Z.; Li, X.; Wu, X.; Brown, N.; Naud, C.; Mayou, D.; Li, T.; Hass, J.; Marchenkov, A. N. *Science* **2006**, *312*, 1191.